CO2 uptake of cement by-pass dust via direct aqueous carbonation: an experimental design for time and temperature optimisation

Materials and Structures (2024) 57:181
https://doi.org/10.1617/s11527-024-02457-0

ORIGINAL ARTICLE

CO_2 uptake of cement by-pass dust via direct aqueous carbonation: an experimental design for time and temperature optimisation

Francesca Bonfante · Pedro Humbert · Jean-Marc Tulliani · Paola Palmero · Giuseppe Ferrara

Received: 13 June 2024 / Accepted: 30 August 2024

Abstract The compositional characteristics of cement by-pass dust (CBPD), specifically its alkalinity and salt content, present significant limitations to its reinsertion in cement production. Furthermore, these characteristics give rise to considerable concerns regarding its disposal. The present study investigated the potential for treating CBPD through the application of a direct aqueous carbonation technique. The aim is to assess carbon capture potential of the material and to investigate the impact of the mineralisation process on its composition. The process was conducted under atmospheric pressure, at low temperature (20–60 °C) and for short duration (20–60 min). Different CO_2 quantification techniques were employed to assess experiments efficiency and replicability of the adopted quantification techniques. A Design of Experiment was developed to identify the optimum carbonation conditions in terms of time and temperature. The conditions for CO_2 content maximisation resulted in a fair agreement with the prediction of the response surface methodology. High values in CO_2 uptake (25.1%) and carbonation degree (82%) were achieved, outperforming previous literature studies. Moreover, the mineralisation process significantly reduces the chloride content of CBPD, paving the way for its adoption as a supplementary cementitious material in integrated industrial processes for carbon capture and utilisation.

Keywords Carbon capture and utilisation · Cement by-pass dust (CBPD) · Direct aqueous carbonation · CO_2 uptake

1 Introduction

It is estimated that approximately 40% of global energy resources are currently being exploited in the construction industry [1]. In this context, cement represents the most widely used building material, and its production is continuously increasing in order to meet the extensive global demand for housing and infrastructure construction. It was estimated that production increased by approximately 7% compared to 2012 and by approximately 50% compared to 2003 [2, 3]. In addition, the production of ordinary Portland cement (OPC) represents a significant source of anthropogenic carbon emissions into the atmosphere. In 2021, the sector provided a substantial contribution of 1.7 billion metric tons as direct emissions to the global CO_2 inventory [4]. Furthermore, cement plants generate considerable quantities of waste in the form of dust on an annual basis, with Europe and

F. Bonfante · J.-M. Tulliani · P. Palmero · G. Ferrara (✉)
INSTM R.U. Lince Laboratory, Department of Applied Science and Technology, Politecnico di Torino, Corso Duca Degli Abruzzi 24, 10129 Turin, Italy
e-mail: giuseppe.ferrara@polito.it

P. Humbert
CRH Innovation EMAT, De Klencke 10-12, 1083 HL Amsterdam, The Netherlands

Published online: 16 September 2024

the United States of America accounting for millions of tons [5]. These dusts, classified as cement kiln dust (CKD) and cement bypass dust (CBPD), are collected in the rotary kiln and the calcination tower (preheater), respectively. The primary distinction between CKD and CBPD is in their respective compositions. In comparison to CKD, CBPD exhibits a higher calcium oxide content and is notably rich in alkalis, chlorides, and sulphates. The high alkalinity and chloride content, which have been reported to range from 7.5 to 21.9% [6–8], preclude its complete reinsertion within the same cement production process. The chloride content limit is fixed at 0.1% by the EN 197-1 standard [9]. These characteristics also give rise to significant concerns regarding its disposal. Consequently, previous studies have sought to identify potential reuse opportunities, including its use as a soil stabiliser [10], as a filler in asphalt mixtures [11], as a binder for waste stabilisation [12], or as a source for potassium chloride production [13].

Sipple and Mullner [13] proposed a solution based on the separation of chlorides obtained through CBPD washing in water and subsequent filtration. The cleaned dust was subsequently employed as supplementary cementitious material (SCM). Although the process demonstrated encouraging outcomes with regard to CBPD reuse, the chemical procedure entailed the use of reagents such as soda and hydrochloric acid, which significantly reduced any positive environmental impact. However, the alkaline composition of CBPD provides a potential pathway for more strategic applications, such as mineral carbonation through accelerated processes. Accelerated carbonation involves the reaction of alkaline compounds with CO_2, ideally derived from the flue gas of the same plant or reproduced at laboratory scale with pure CO_2 gas, to produce stable mineralised products [14]. The utilisation of a cement by-product as a sink for carbon sequestration simultaneously contributes to carbon and waste cycling, thereby facilitating the decarbonisation of the cement industry in a virtuous circular economy approach. Consequently, cement dust has been employed in recent studies examining the carbon capture capacity. Huntzinger et al. [15, 16] demonstrated that a substantial carbonation rate can be attained when employing CKD, even under ambient pressure and temperature conditions. Araizi et al. [17] investigated the accelerated carbonation of several industrial wastes. They observed that CBPD exhibited a notable degree of carbonation due to its calcium oxide-rich composition, and that sonication enhanced the efficiency of the mineralisation process. However, these applications did not assess the effectiveness of the process in removing salt content. Moreover, while the impact of temperature on accelerated aqueous carbonation has been extensively examined with various industrial waste and by-product materials, often demonstrating a substantial influence [18, 19], this particular aspect has not been subjected to a comprehensive analysis in the context of cement dust. Furthermore, the literature on mineral carbonation processes is not homogeneous. Different techniques are used to carry out accelerated carbonation, and different methods are employed to quantify CO_2 levels. This necessitates the verification of the reliability of some common quantification techniques.

The present study aims at showing the path to increase carbon capture capacity of cement by-pass dust, and at the same time to analyse the efficiency in terms of salt removal in a single step process avoiding any pre-treatment of the material. In order to achieve this, the CBPD was selected in preference to CKD, which typically exhibits a lower chloride content. A direct aqueous carbonation route was adopted for the mineralisation, which was identified as very promising for the carbonation of industrial waste [20], but up to now, it has scarcely been applied to CBPD. The influence of temperature, in conjunction with the duration of carbonation, was investigated in order to develop a model for optimising the operational parameters of the mineralisation process. Furthermore, the replicability of the experiments and the reliability of certain quantification techniques were evaluated.

2 Materials and methods

2.1 Material characterisation

Cement bypass dust (CBPD) powder was supplied by a cement plant based in Ireland. The particle size distribution was determined by laser granulometry (Malvern Mastersizer 3000 AERO S, Worcestershire, UK), and the results are presented in Fig. 1. The D_{10}, D_{50} and D_{90} values, as determined by the cumulative

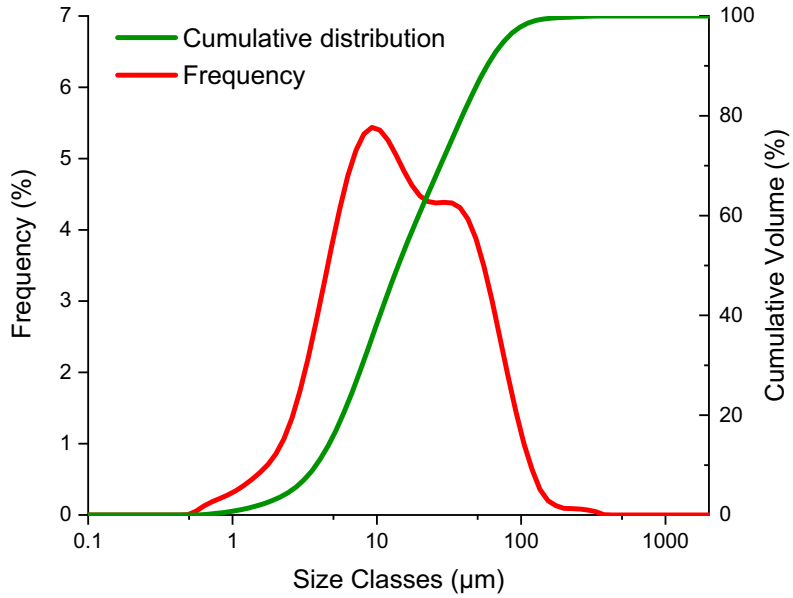

Fig. 1 Cumulative and Frequency curves of as-received CBPD powder

curve distribution, were found to be 3.79 μm, 14.1 μm and 58.0 μm, respectively.

The mineralogical composition of as-received and carbonated CBPD was investigated through X-ray diffraction analysis (XRD, Empyrean Malvern Panalytical, Almelo, The Netherlands) in Bragg–Brentano configuration, with Cu-Kα wavelength radiation (0.15406 nm) operating at 40 kV and 40 mA. 2θ spanned from 5to 70 ° with an angular step of 0.006 ° held for 23 s. The diffractometer was equipped with soller slits (0.04 rad), anti-scatter slit (P7.5), beam mask (10 mm), divergence (¼ °) and axial (½ °) slits. Field-emission Scanning Electron Microscopy (FESEM, Hitachi S4000, Tokyo, Japan) was used to analyse the powder morphology before and after the carbonation.

An X-ray fluorescence (XRF) spectrometer (Rigaku, Supermini200, Tokyo, Japan) was employed to evaluate the chemical composition of the samples. The most abundant elements in the powder, as expressed in oxide form, were calcium, potassium and silicon (Table 1). Additionally, a considerable quantity of chlorine was identified, which is a common constituent of CBPD waste material.

It is possible to calculate the carbonation potential ($ThCO_2$) according to Eq. (1), based on the chemical composition of the material. This equation, based on the Steinour formula, which was originally conceived for the assessment of carbonation potential in mortar and concrete [21], was subsequently adapted by Huntzinger et al. [15] for use with generic materials. The equation assumes that all CaO (except calcium already bound in $CaSO_4$ and $CaCO_3$) will form calcium carbonate, MgO will form magnesium carbonate, and Na_2O and K_2O (except the one bound in sylvite, KCl) will form Na_2CO_3 and K_2CO_3, respectively. The value of $\%CaCO_3$ was derived from the CO_2 content of the as-received material (discussed in paragraph 3.2). The value of %KCl was derived from XRF data assuming that the entire potassium content is related to chlorine to form KCl (%KCl = 26.7 wt.%).

$$\begin{aligned}\%ThCO_2 = {} & 0.785\left(\%CaO - 0.56 \cdot \%CaCO_3 - 0.7 \cdot \%SO_3\right) \\ & + 1.091 \cdot \%MgO + 0.71 \cdot \%Na_2O \\ & + 0.468(\%K_2O - 0.632 \cdot \%KCl)\end{aligned} \quad (1)$$

Table 1 As-received cement bypass dust chemical composition (% wt)

Oxides	CaO	K_2O	Cl	SiO_2	SO_3	Al_2O_3	Na_2O	Fe_2O_3	MgO	Other	LOI-Flux
(%)	39.10	16.90	14.80	5.85	2.61	2.11	1.84	1.45	1.11	0.83	13.40

According to Eq. (1), CBPD carbonation potential resulted in 30.5%.

2.2 Aqueous carbonation set-up

The aqueous carbonation of CBPD was conducted in a 500 mL flask. The flask was filled with the slurry, which consisted of cement bypass dust suspended in distilled water at room temperature and was homogenised through continuous magnetic stirring. CO_2 was introduced into the flask at a constant flow rate and ambient pressure, as measured by a flowmeter. To prevent the formation of a pressurised system, the flask was partially closed with a drilled cap, allowing for the insertion of the CO_2 pipe. The experiments were conducted in a suction hood.

The experiments were conducted under standard atmospheric pressure conditions. The slurry was prepared with a liquid-to-solid ratio (L/S) of 3, whereby 100 g of CBPD was added to 300 g of deionised water. The magnetic stirrer was set at 1200 rpm, and the CO_2 flow rate was maintained at 150 L/h. The CO_2 purity in the gas cylinder was 99.9% (grade 2.5, SIAD, Turin, Italy). The pH was measured at the outset and at the conclusion of the carbonation process. The initial pH was approximately 13, and it decreased to approximately 10 at the end of the experiment. After carbonation, the solid fraction of the slurry was separated from the liquid by centrifugation for 4 min at 3000 rpm (REMI equipment). Subsequently, the powder was subjected to a drying process at 60 °C for approximately 24 h until a constant weight was attained. The adopted L/S ratio permitted the simultaneous carbonation and hydration of the powder during the aqueous mineralisation process. To gain a deeper understanding of the impact of carbonation, samples that underwent only hydration were produced for comparison. The hydrated samples were prepared with the aforementioned operational parameters, excluding the fluxing of CO_2. To confirm the reproducibility of the experiment, three carbonation tests were conducted under identical conditions, specifically at room temperature and with a reaction time of one hour. The CO_2 content of each sample after carbonation was measured three times with each quantification technique.

2.3 Design of experiment

The study investigated the effects of reaction time and temperature with the perspective of optimising the mineral carbonation process. To this end, a Design of Experiments (DoE) was developed using Minitab (version 20.1.3). The experiments were designed using Response Surface Methodology (RSM). RSM involves the execution of a fixed number of experiments, the objective of which is to ascertain the effect of independent variables on the system response. The objective of this approach is to reduce the amount of information required by conducting a minimum number of experiments [22]. A Central Composite Design (CCD) was selected to create an experimental design space consisting of two operational parameters: reaction time (min) and temperature (°C). The remaining parameters were maintained in accordance with the specifications outlined in the preceding paragraph. In selecting the experimental ranges, the maximum reaction time was set based on the initial results, which demonstrated the complete conversion of the reactive phases within one hour. With regard to the temperature, it should be noted that the open system adopted in this study would have resulted in the evaporation of the slurry at temperatures exceeding 60 °C. Accordingly, the adopted experimental ranges were 20–60 min and 20–60 °C. RSM generated a set of 11 experiments to analyse the individual and combined effects of the operating parameters on the CO_2 final content.

2.4 CO_2 quantification methods

In order to quantify the CO_2 content of carbonated samples, three different testing procedures, previously defined by the authors in a separate study [23], were employed: (i) thermogravimetric analysis (TGA), (ii) thermal decomposition carried out in a muffle furnace and (iii) acidic digestion. The first two methods determine the CO_2 content according to the same principle: the thermal decomposition of calcium carbonate is an endothermic reaction that yields calcium oxide and carbon dioxide (Eq. 2).

$$\begin{aligned} &CaCO_{3(s)} \rightarrow CaO_{(s)} + CO_{2(g)} + \Delta H \\ &\Delta H = -178\left[\mathrm{kJ/mol}\right] \end{aligned} \quad (2)$$

It is assumed that the complete reaction of calcium carbonate decomposition occurs within a temperature range of 550to 850 °C, in accordance with the findings of similar studies referenced in the literature [24–30]. Therefore, Eq. (3) is typically employed for the calculation of CO_2 content, on the assumption that the total weight loss is attributable to carbonate decomposition. It was assumed that any potential weight loss from hydrated phases within the specified temperature range would be negligible.

$$m_{CO_2}(\%) = \frac{(m_{550^\circ C} - m_{850^\circ C})}{m_i} \times 100 \quad (3)$$

In which m_i represents the initial mass of the measured sample, while $m_{550\ ^\circ C}$ and $m_{850\ ^\circ C}$ are the mass of the sample after heating at 550–850 °C, respectively.

The dried powder was subjected to simultaneous thermogravimetric-differential thermal analysis (TG–DTA) using the LABSYS EVO system from Setaram (Caluire, France). The heating cycle comprised an initial isotherm at 30 °C for five minutes, followed by a heating ramp to 1050 °C at 10 °C/min, and then a cooling ramp to 30 °C at the same rate. The test was conducted with nitrogen serving as the purge gas (20 mL/min), and the tested samples had a mass of 50 mg.

Thermal decomposition is a two-stage process conducted in a muffle furnace, comprising a preliminary thermal treatment up to 550 °C and a subsequent one up to 850 °C. This technique offers the possibility of obtaining similar information regarding the content of CO_2 when compared to TGA but utilises simpler and less expensive equipment. In the case of thermal decomposition, it is possible to maintain the use of Eq. (3) by considering the initial mass of the powder (m_i) and the weights of the samples ($m_{550\ ^\circ C}$ and $m_{850\ ^\circ C}$) recorded after the thermal treatments. These samples are composed of the tested powder placed in an alumina crucible and their weights are obtained after the completion of the thermal treatments [23, 31]. The initial mass tested was approximately 3 ± 0.5 g. Thermal decomposition measurements were conducted on three samples for each investigated configuration.

The acid digestion methods assume that the carbon dioxide content is equal to the mass loss of the dry sample when subjected to a dilute hydrochloric acid solution [23, 32]. The assumption is that the gaseous phase liberated during acid digestion is composed entirely of carbon dioxide, and that all carbonates react with hydrochloric acid, producing CO_2 in accordance with Eq. (4).

$$CaCO_{3(aq)} + 2HCl_{(aq)} \rightarrow CaCl_{2(aq)} + CO_{2(g)} + H_2O_{(l)} \quad (4)$$

The experiment is conducted in a 250 mL flask containing 100 mL of diluted HCl solution (0.001 M) and 5 g of powder. The mass of the system is recorded at regular five-minute intervals until a constant mass is achieved, which typically occurs within 20 min. The CO_2 content is calculated in accordance with the following equation:

$$CO_2(\%) = \frac{(m_0 - m_f)}{m_i} \times 100 \quad (5)$$

where m_0 is the initial mass of the system, m_f is the final mass of the system and m_i is the initial mass of powder.

2.5 CO_2 uptake definition

To quantify the carbon uptake of materials, different studies [15, 33, 34] agree with the calculation of the CO_2 uptake as the quantity of CO_2 captured (ΔCO_2) referred to the initial mass of the material (m_i), as defined in Eq. (6).

$$\%CO_{2\ \text{uptake}} = \frac{\Delta CO_2}{m_i} \cong \frac{\%CO'_{2\ \text{content}} - \%CO_{2\ \text{initial}}}{1 - \left(\%CO'_{2\ \text{content}}\right)} \quad (6)$$

$$\%CO'_{2\ \text{content}} = m_{CO_2 - \textit{after carbonation}}$$

$$\%CO_{2\ \text{initial}} = m_{CO_2 - \text{before carbonation}}$$

In Eq. (6), $\%CO'_{2\ \text{content}}$ represents the carbon content after carbonation, whereas $\%CO_{2\ \text{initial}}$ denotes the initial carbon dioxide content of the raw material. This equation is based on the assumption that the mass changes observed after carbonation are solely attributable to the capture of CO_2 by the material. Nielsen and Quaghebeur [35] demonstrated that the neglect of mass changes resulting from de-hydroxylation and/or hydration reactions can lead to a significant under- or overestimation of

the effective CO_2uptake. With regard to CBPD, it was evident that considerable mass alterations were attributable to hydration processes and chloride dissolution during the aqueous carbonation procedure, which subsequently underwent removal through centrifugation. These mass changes (Eq. 7) were found to be non-negligible in the CBPD under analysis (see paragraph 3.4). Therefore, Eq. (6) was modified to yield Eq. (8)

$$m_{carb} = m_i + \left(m_{CO_{2carb}} - m_{CO_{2initial}}\right) + \Delta m \tag{7}$$

$$\%\,CO_{2\,\text{uptake}} = \frac{\Delta CO_2}{m_i} \cong \frac{\%CO'_{2\,\text{content}} \times \left(1 + \frac{\Delta m}{m_i}\right) - \%CO_{2\,\text{initial}}}{1 - \left(\%CO'_{2\,\text{content}}\right)} \tag{8}$$

where Δm represents mass changes other than those due to captured CO_2 and m_i the initial mass of as-received material.

The increase in the mass of hydration was quantified through TGA and thermal decomposition in the range 60–350 °C. The removed mass of salt was determined by collecting and drying the supernatant from the separated slurry, which was obtained by centrifugation. In this study, Eqs. (6) and (8) were adopted and compared.

The carbonation degree, denoted as η_{ca}, was defined as the amount of CO_2 captured with respect to the theoretical maximum extent of carbonation (Eq. 9).

$$\eta_{ca}(\%) = \frac{\%\,CO_{2\,\text{uptake}}}{ThCO_2} \cdot 100 \tag{9}$$

3 Results and discussion

3.1 Influence of carbonation upon phase composition

The composition of CBPD was analysed through XRD analysis before carbonation, after hydration and after carbonation (Fig. 2). The peaks of higher intensity related to the main phases involved in the reactions, were highlighted in the figure to emphasise the changes in the material composition due to hydration and carbonation processes. The mineral composition of the as-received CBPD was found to consist primarily of free lime (CaO) and halite/sylvite ($K_{0.7}Na_{0.3}Cl$). Additionally, other compounds that are typically present in the composition of cement and related waste materials were identified, including portlandite ($Ca(OH)_2$, CH), quartz (SiO_2), dicalcium silicate (Ca_2SiO_4), tricalcium silicate (Ca_3SiO_5), mayenite ($Ca_{24}Al_{27}FeO_{67}Cl_{2.50}$) and anhydrite ($CaSO_4$). The presence of portlandite, even with a low peak intensity, indicates that the free lime present in the raw material was partially hydrated as a result of weathering conditions. The hydrated powder exhibited a considerable quantity of calcium hydroxide, which was formed during the hydration of lime. Additionally, the main calcium carbonate peak increased, likely due to the natural carbonation of portlandite during the drying phase. Furthermore, the hydration process resulted in the formation of hydrocalumite ($Ca_4Al_2(OH)_{12}(Cl,CO_2,OH)_2{\cdot}4H_2O$) [36] and gypsum. The presence of mayenite and dicalcium silicate was identified both prior to and following the hydration process. In the carbonated powder, the carbonation reaction led to the complete consumption of lime and portlandite, which actively contributed to the formation of calcium carbonate. After the aqueous carbonation, the disappearance of tricalcium silicate may be attributed both to carbonation and the hydration reaction, forming calcium silicate hydrate (C-S–H) gel, not detectable through XRD analysis being an amorphous or poorly crystalline phase. Mayenite was not detected after carbonation, suggesting its involvement in the reaction. Instead, quartz and dicalcium silicate peaks were still detected after carbonation. The carbonated powder did not exhibit any indications of gypsum, however, a distinct phase in combination with potassium, langbeinite, was identified. The diminution in the intensity of the sylvite peaks is attributed to the dissolution of KCl within the aqueous slurry, which then underwent a process of separation from the powder through the application of centrifugation.

TG–DTA allowed the identification and quantification of the various compounds present in the sample. As illustrated in Fig. 3, the DTA curves of the as-received (yellow line), hydrated (blue line) and carbonated (green line) powders reveal the existence of three distinct regions. The first region (*i*), spanning from room temperature to 350 °C, is characterised by the removal of free and bound water, and associated with the decomposition of C-S-H compounds. The second region *(ii)* is linked to the dehydroxylation of

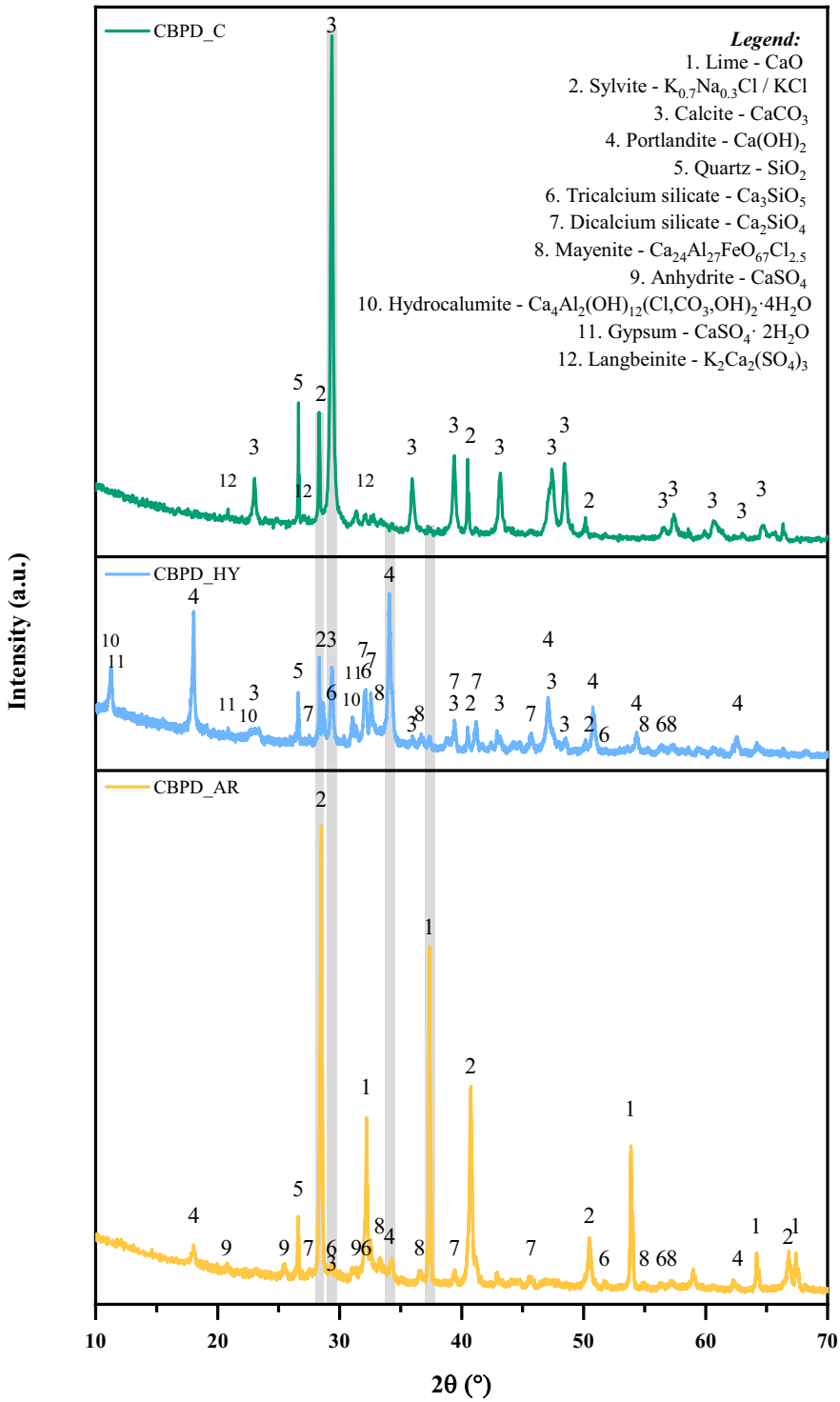

Fig. 2 XRD pattern of as-received (CBPD_AR), hydrated (CBPD_HY) and carbonated (CBPD_C) CBPD (Index codes of the different phases: 1. 96-900-8606; 2. 96-900-3180/96-900-3122; 3. 96-702-2028; 4. 96-100-1788; 5. 96-900-9667; 6. 96-154-0705; 7. 96-901-2794; 8. 96-901-5595; 9. 96-500-0041; 10. 96-900-9354; 11. 96-101-0982; 12. 96-9005789)

the portlandite phase. The third region (*iii*) is typically associated with the decomposition of calcium carbonates [37].

The as-received powder exhibited a significant peak in the second temperature region, at 445 °C (peak IV), corresponding to the dehydroxylation

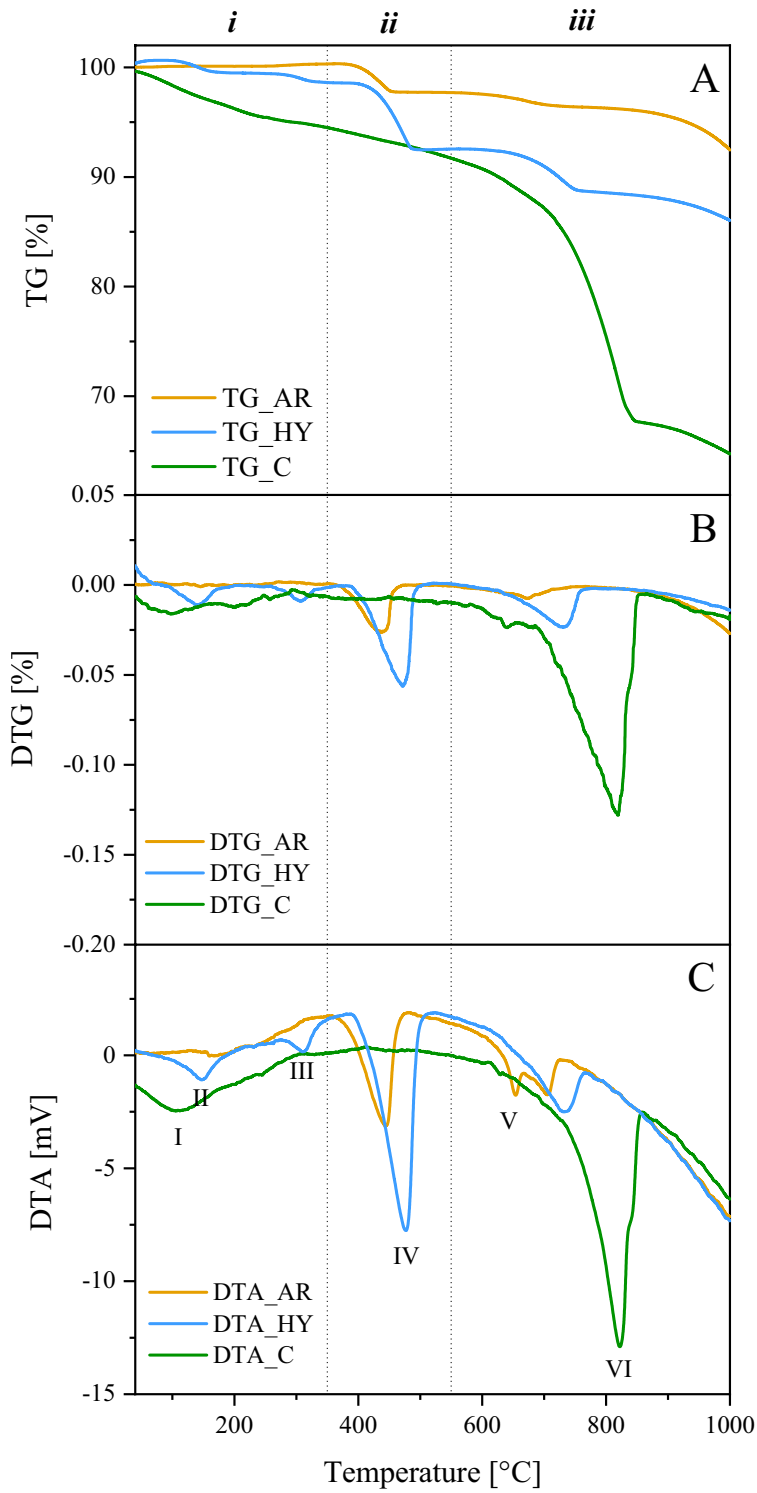

Fig. 3 TG (**A**), TG derivative (**B**) and DTA (**C**) curves of cement bypass dust as-received (yellow), hydrated (blue), carbonated (green)

of calcium hydroxide, estimated to be equal to 10.6% w/w, which is consistent with the XRD analysis. The third range was distinguished by the presence of two peaks, occurring at 650 °C (peak V) and 700 °C (peak VI). Peak V is specifically associated with the melting of potassium and sodium chloride (KCl-NaCl) [38]. The mass loss associated with peak V was approximately 0.6%, indicating that the contribution of salt melting can be considered negligible with respect to the mass loss due to calcium carbonate decomposition (peak VI).

In the hydrated sample, peak II, occurring at approximately 140 °C, is associated with gypsum dehydration. However, peak II, together with peak III, which occurs at about 315 °C, also confirmed the presence of AFm phase (hydrocalumite), which has previously been shown to decompose at about 310 °C [36, 39]. Region *ii* was distinguished by an intense signal attributed to portlandite (peak IV), with a content of 24.5% w/w. In the third region, a signal indicative of calcium carbonate decomposition (peak VI) was observed. However, no peak corresponding to the melting of chloride salts (KCl, NaCl) was detected, confirming a lower content compared to the as-received powder.

In regard to the carbonated powder, the initial region of differential thermal analysis (DTA) exhibited a broad endothermic signal at approximately 100 °C (peak I). However, the peaks associated with hydrocalumite, which were present in the hydrated powders, were not detected. Indeed, the stability of hydrocalumite is pH-dependent, and the aqueous carbonation, which lowered the pH, prevented its formation [40, 41]. Peak I is typically associated with the dehydroxylation of C-S–H, which corresponds to a mass loss typically observed between 60 °C and 350 °C, in addition to a potential release of free water. A comparison of the TG curves in region *i* reveals a distinct difference between the hydrated and carbonated materials. While the hydrated powder exhibited a limited weight loss up to 350 °C, the carbonated material demonstrated a continuous and significant mass loss within the same temperature range, indicating an increased extent of hydration during the carbonation process. These findings are consistent with those of a previous study [42], which reported that the quantity of hydration products formed during the carbonation of calcium silicates was greater than that produced during hydration under identical conditions, although exhibited a lower Ca/Si ratio.

In the third region, a substantial endothermic signal (peak VI) was identified within the temperature range of 550–850°C, thereby confirming the successful occurrence of the carbonation reaction. The shift of peak VI (related to carbonate decomposition) to higher temperatures for hydrated and carbonated CBPD is commonly associated with an increased calcium carbonate content. The calcium hydroxide formed in the slurry was entirely consumed during the carbonation reaction, resulting in the formation of calcium carbonates. This is evidenced by the almost flat DTA curve observed in the second region.

Scanning electron microscopy (SEM) observations were conducted on the as-received and carbonated samples at varying magnifications (Fig. 4). The as-received material exhibited the presence of multiple cubic-shaped grains, with a size range of 2–5 µm (Fig. 4a), which may be associated with the potassium chloride salt. In studies on the hydration of CBPD, it was found that when a high quantity of sylvite was present, the hydrated powder was primarily covered by partially dissolved KCl, which may impede the identification of other phases [43, 44]. Nevertheless, at higher magnifications (Fig. 4c), it was possible to observe hexagonal crystals associated with portlandite, in addition to fine (submicrometric, with rounded shape) CBPD particles forming micrometric agglomerates.

A significantly different morphology was observed in the carbonated powder, wherein the particles exhibited a more wrinkled surface and were covered by ultrafine precipitates (Fig. 4b). Oral et al. [45] synthesized calcium carbonate particles via precipitation reaction between calcium acetate and sodium bicarbonate and investigated the influence of pH and $[Ca^{2+}]$:$[CO_3^{2-}]$ ratio on calcium carbonate morphology. In the case of a lower ratio of calcium ions to bicarbonate ions, calcite polymorphs were observed to assume a smaller size and a spheroidal shape. Accordingly, the spheroidal morphologies observed on the particles were associated with nanometric (100–200 nm) calcium carbonate precipitates, given the high concentration of CO_2 present in the carbonation process.

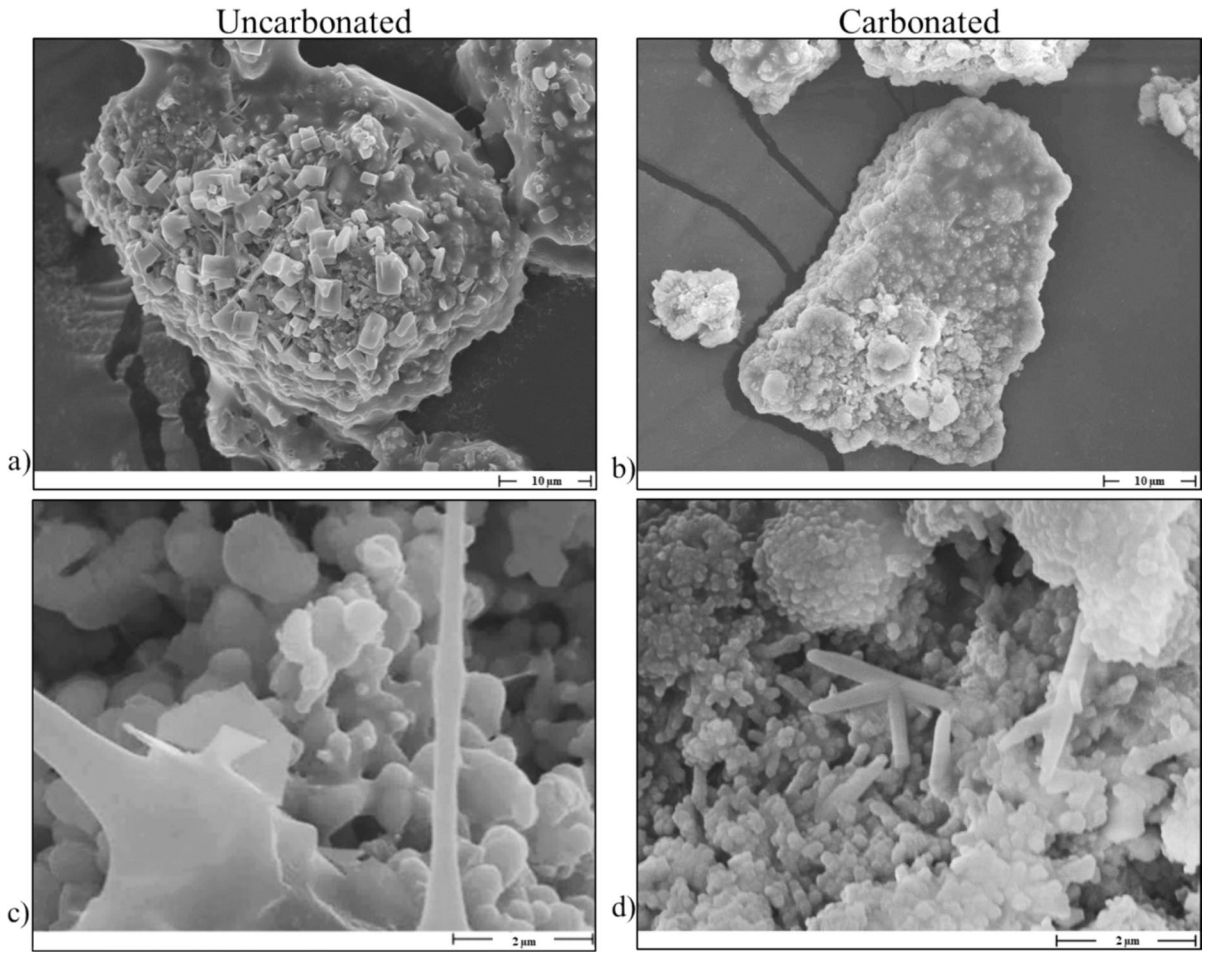

Fig. 4 SEM images of CBPD as-received (**a** and **c**) and carbonated (**b** and **d**)

3.2 Experiment replicability

Figure 5 illustrates the CO_2 contents obtained from different quantification techniques for the as-received (CBPD_AR) and hydrated (CBPD_HY) powders, as well as for the three carbonated replicates (CBPD1, CBPD2 and CBPD3). The values were calculated using the formulas provided in Eqs. (3) and (5). The third replicate (CBPD3) was subjected to three measurements for each of the techniques. The error bars displayed in the chart (Fig. 5) represent the standard deviation. The coefficient of variation was calculated as the ratio between the standard deviation and the average of the measurements from CBPD3. It was approximately 12% for TGA and acid digestion and approximately 5% for thermal decomposition.

The hydrated CBPD exhibited a higher CO_2 content than the as-received powder, which can be attributed to the natural carbonation of the sample occurring during the drying step subsequent to hydration. The hydrated sample contains considerable quantities of calcium hydroxide, which is highly reactive with atmospheric CO_2 and naturally forms calcium carbonate when exposed to air. Furthermore, the CO_2 content values obtained through thermal decomposition for both the as-received and hydrated CBPD powders were higher than those determined through the other quantification techniques. These discrepancies can be attributed to the natural carbonation of calcium hydroxide that occurs during the prolonged heating and cooling cycles in the muffle furnace, which are not present in the other techniques. Accordingly, the CO_2 contents of CBPD_AR and CBPD_HY were

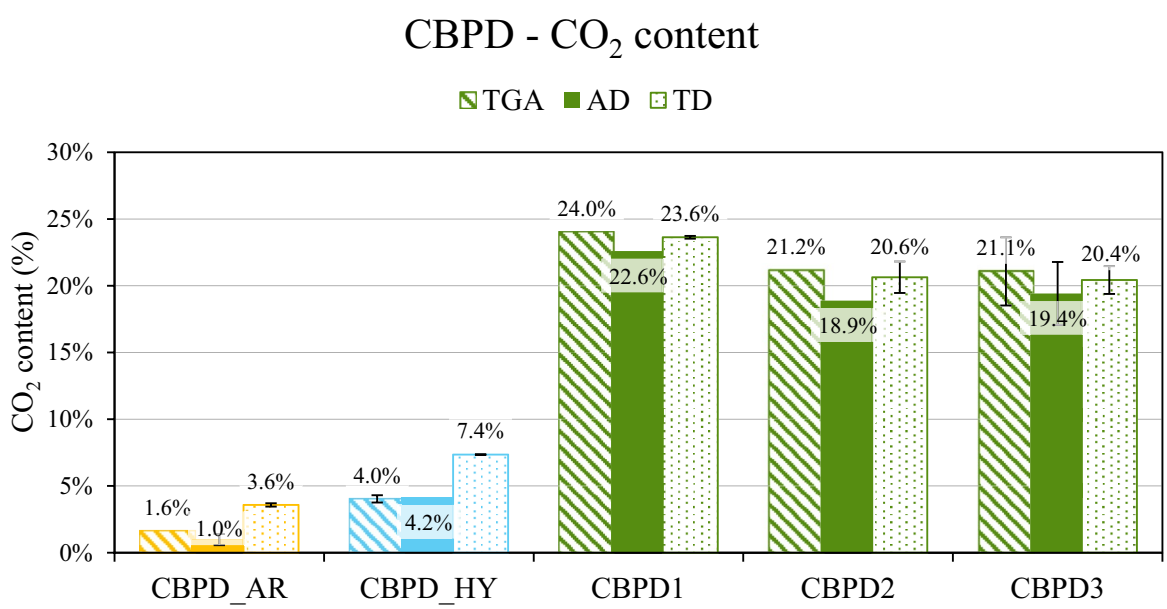

Fig. 5 Carbon content quantification throughh Thermogravimetric Analysis (TGA), Acid Digestion (AD) and thermal Decomposition (TD). Legend: cement bypass dust as-received (CBPD_AR), hydrated (CBPD_HY), carbonated (three replicates: CBPD1, CBPD2, CBPD3)

calculated without incorporating the thermal decomposition method. In contrast, the results obtained from the carbonated powders can be regarded as unaffected by this phenomenon, given that the material was previously subjected to accelerated carbonation. Therefore, the reactive phases were fully consumed. An analysis of variance (ANOVA) was conducted using the general linear model, based on both replicates of the carbonation test and CO_2 quantification techniques. The ANOVA indicated that there were no statistically significant variations in the quantification techniques (p value = 0.279), thereby demonstrating the interchangeability of TGA, acid digestion and thermal decomposition for CO_2 quantification. These findings corroborate those of the preceding study by Ferrara et al. [23], thereby substantiating the dependability of the CO_2 quantification techniques employed. With regard to the statistical analysis of the replicates of the carbonation test, a notable degree of variability in the results was observed (p value = 0.042). In particular, while the estimates of CBPD2 and CBPD3 (respectively with an average CO_2 content of 20.2% and 20.3%) are quite similar, a higher degree of variability is observed when comparing with the CBPD1 value (23.4%). However, while the CBPD2 and CBPD3 tests were conducted at approximately the same time, the CBPD1 test was performed a few months earlier at a higher room temperature (of about 26 °C), due to seasonal variations, that has increased the reactivity of the material. It is therefore reasonable to conclude that the observed variability between CBPD1 and CBPD2-3 is attributable to changes in room temperature.

3.3 Carbonation optimisation: effect of time and temperature

The study investigated the effect of time and temperature on carbonation using Response Surface Methodology (RSM). The CO_2 content was determined exclusively through acid digestion, as this is the most expedient of the three techniques investigated, particularly when a substantial number of experiments are conducted. The impact of time and temperature has been extensively examined in the existing literature and across a range of materials. It is anticipated that the CO_2 content will increase over time until reaching a plateau, which indicates the saturation of the material available for the carbonation reaction. Additionally, the impact of elevated temperatures, particularly within pressurised environments, is understood to enhance CO_2 uptake. In

Table 2 Design of experiment observations

Obs	Uncoded units		Coded units		
	T(°C)	t(min)	X-T(°C)	Y-t(min)	CO_2 content (%)
CBPD3	20.00	60.00	−1.00	1.00	19.42
CBPD4	20.00	20.00	−1.00	−1.00	15.48
CBPD5	40.00	40.00	0.00	0.00	20.71
CBPD5B	40.00	40.00	0.00	0.00	23.27
CBPD6	60.00	20.00	1.00	−1.00	17.57
CBPD7	60.00	60.00	1.00	1.00	20.83
CBPD8	11.72	40.00	$-\sqrt{2}$	0.00	18.83
CBPD9	40.00	11.72	0.00	$-\sqrt{2}$	15.79
CBPD10	68.28	40.00	$\sqrt{2}$	0.00	14.44
CBPD11	40.00	68.28	0.00	$\sqrt{2}$	24.09
CBPD12	40.00	60.00	0.00	1.00	23.21

the experimental configuration proposed by the present study (open system), an increase in temperature is expected to lead to two opposing effects. While higher temperatures improve the reaction kinetics of calcium dissolution and, therefore, its availability for the carbonation reaction, they reduce the solubility of CO_2 in the slurry. Thus, an arc trend is expected to describe the effect of temperature, the trajectory of which depends on the specific kinetic of the studied material. Table 2 lists the results of the observations taken following the CCD and obtained as the average of three repeated measurements. CBPD12 was identified as the point of the suggested maximum. Figure 6 shows the experimental observations and the relative curve predicted by the model. From these data, the interaction plots confirmed the expected trajectories for time and temperature (Fig. 6).

The most suitable model was selected based on the evaluation of R^2 adjusted, residual plots and the

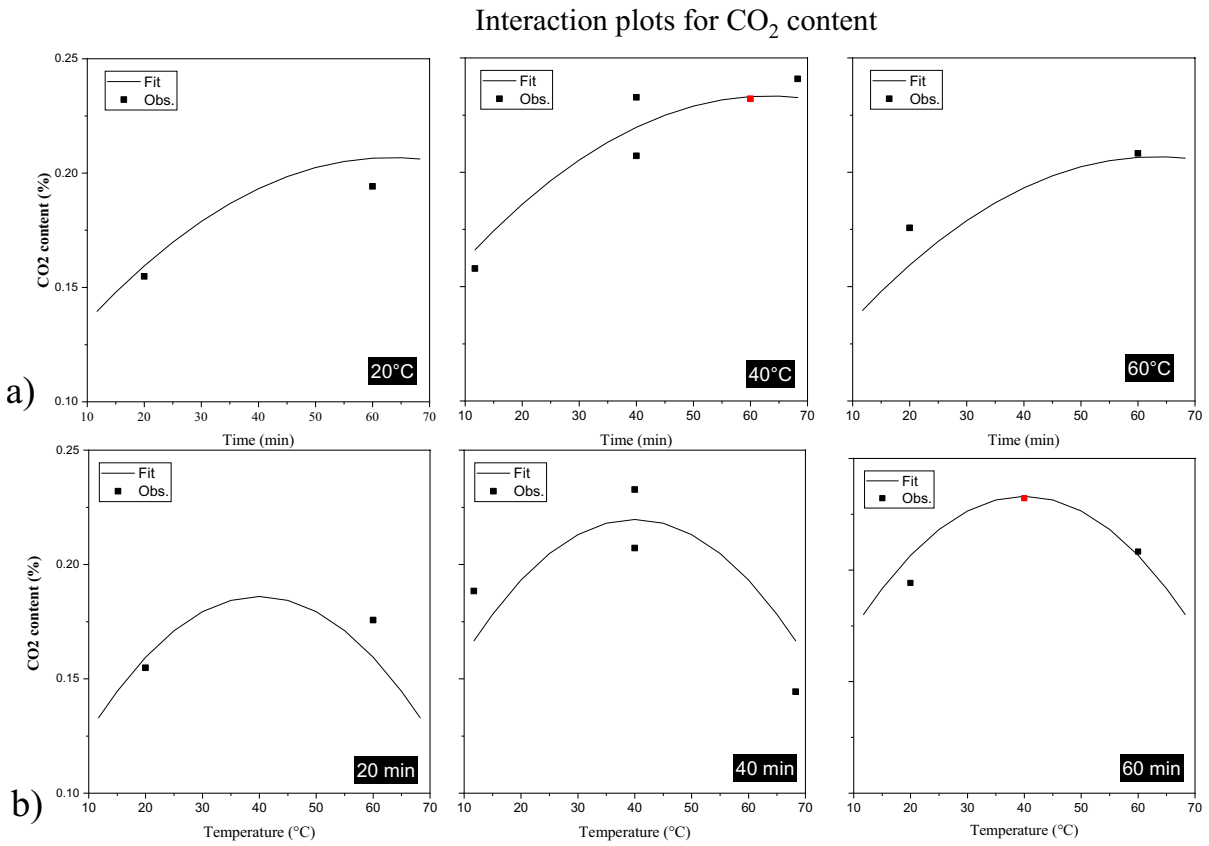

Fig. 6 Interaction plots describing temperature (**a**) and time (**b**) effects on CO_2 content. The prediction lines are coupled with the observations (in black) and the optimum point (in red)

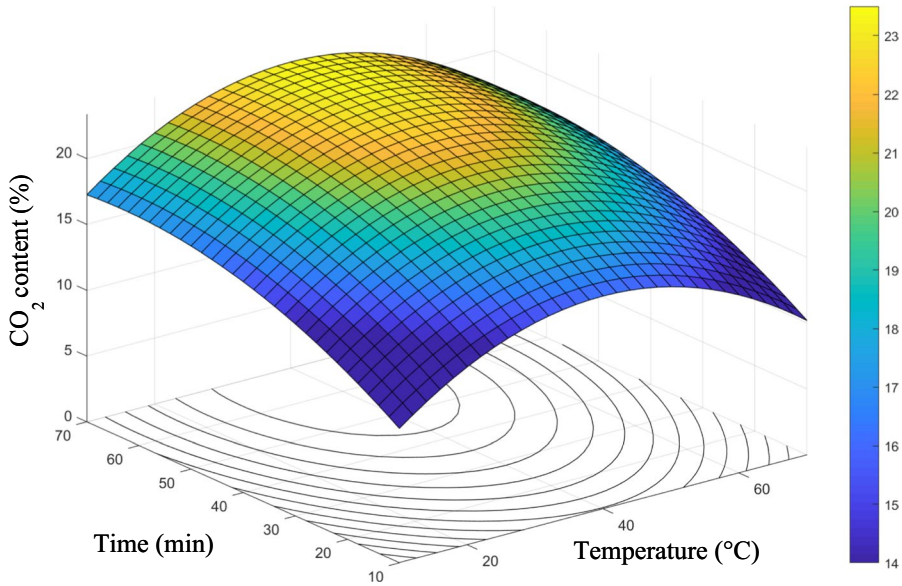

Fig. 7 Surface plot of the combined effect of time and temperature on CO_2 content (%)

stepwise method (Fig. 7). This model demonstrated an R^2 value of 83.3% and an S value of 0.0163. The combined effect of time and temperature was found to be negligible, as was the linear effect of temperature. This resulted in the formation of a non-hierarchical model. Accordingly, the model's regression equation (Eq. 10) was solely calculated in coded units, as illustrated in Table 2.

$$CO_2 content\ (\%) = 21.97 + 2.355\ Y - 2.653\ X^2 - 1.015\ Y^2 \quad (10)$$

The recorded CO_2 content exhibited a range of 14.4–24.1%. The model indicated that the optimal conditions would be 40 °C and 63 min, with a CO_2 content of 23.3%. At 40 °C and 60 min, the experimental value was found to be 23.2%, which was highly comparable to the RSM prediction and fell within the confidential interval (standard error of fit = 0.8%). In any case, the CO_2ontent should increase over the course of the reaction in a plateau-like trajectory, as evidenced by the empirical observations (CBPD11). This discrepancy can be attributed to the inherent limitations of the model, including the employment of full quadratic terms, the highly similar standard error and model variance of CO_2 content above 60 min, and the saturation of the reaction close to the experimental limits. Therefore, while the CO_2 content should result in a slight increase over time, the model identifies an optimum point at 63 min. Indeed, extending the reaction time beyond 60 min, does not result in any significant improvement of CO_2 uptake. Instead, this would result in an increase in the energy consumption associated with the process.

3.4 CO_2 uptake and literature comparison

A critical challenge in studying CO_2uptake is the inherent uncertainty associated with changes in mass of CBPD during aqueous carbonation. Nevertheless, this value is fundamental for comparison with existing literature and for the objective evaluation of the experiment's efficiency. Given the difficulty of measuring these data for each experimental point, an investigation into the correct CO_2 uptake was only conducted for the temperature/time combination of 40 °C and 60 min (CBPD12).

Firstly, an evaluation of the influence of these mass changes on the CO_2 uptake based on the CO_2 content was conducted, the results of which are presented in Fig. 8. Equations (6) and (8) were plotted by varying the CO_2 content while maintaining the initial CO_2 concentration at approximately 2%. The inclusion of higher CO_2 contents serves to increase the degree of variation observed in the CO_2 uptake value, which is a consequence of the influence of other mass changes (Δm). In particular, for the selected observation (CO_2 content = 23.2%), the variation in CO_2 uptake estimation could correspond to $\pm 3\%$ for $\Delta m = \pm 10\%$ and $\pm 6\%$ for $\Delta m = \pm 20\%$.

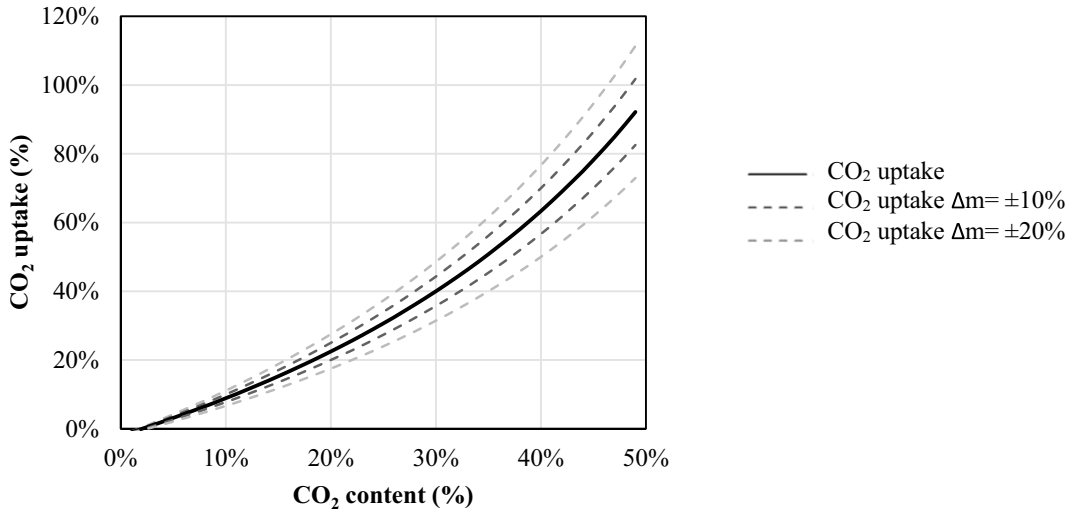

Fig. 8 Influence of mass changes on CO_2 uptake

The quantification of mass changes is related to the increase of initial mass due to hydration reactions and the decrease of initial mass due to the removal of salts at the experimental point CBPD12. The average mass loss resulting from thermal decomposition due to dehydration of hydrated phases was found to be 7%. A residual liquid of 18.5 g was obtained from the centrifugation of the slurry, which was produced with 100 g of as-received CBPD and 300 g of distilled water. Accordingly, the change in mass, Δm, as defined in Eq. (8), was calculated by the sum of the percentage decrease in mass resulting from the separation of salts (–18.5%) and the percentage increase in mass resulting from the hydration of CBPD (7%). The residue was subjected to X-ray fluorescence (XRF) and X-ray diffraction (XRD) analysis to ascertain its chemical composition and confirm the absence of any hydrated phases. The results of the elemental XRF analysis indicated that approximately 90% of the residue was constituted by potassium, sodium, and chlorine. Accordingly, XRD analysis confirmed that the majority of the residue was composed of anhydrous salts, with strong signals belonging to sylvite (KCl) and halite (NaCl), in addition to traces of gypsum and quartz phases (see Fig. 9).

Upon calculation with the modified formula (Eq. 8), the CO_2 uptake was determined to be 25.1%, while the general equation (Eq. 6) would have suggested a CO_2 uptake of 28.5%.

The carbonation degree (η_{ca}) at 40 °C and 60 min of CBPD was approximately 82%.

Table 3 presents a comparison with existing literature on similar aqueous and wet carbonation processes of CBPD and CKD. Gunning et al. [46] observed that CKD exhibited inferior performance, as evidenced by lower CO_2 uptake and carbonation degree, relative to CBPD subjected to carbonation under identical operational parameters. The present study and that of Araizi et al. [17] were conducted under ambient pressure, although with different CO_2 flow rates. In contrast, Gunning et al. [46] conducted their experiments in a closed and pressurised system, and thus, the data pertaining to the CO_2 flow rate are not accessible. As illustrated in Table 3, elevated temperatures and pressures have a beneficial impact on carbonation efficiency. The initial aspect has already been analysed and discussed in this study; however, the effect of pressure could be considered for future perspectives on CO_2 uptake optimisation. Despite the use of different operational parameters, the carbonation degrees attained by this study were markedly superior to those reported in the literature, particularly when compared to results obtained at room temperature. This discrepancy can be attributed to the enhanced reactivity of the powder employed in this study. In analogous conditions, Araizi et al. [17] observed a higher CO_2 uptake for a higher L/S ratio. Nevertheless, while Chang et al.

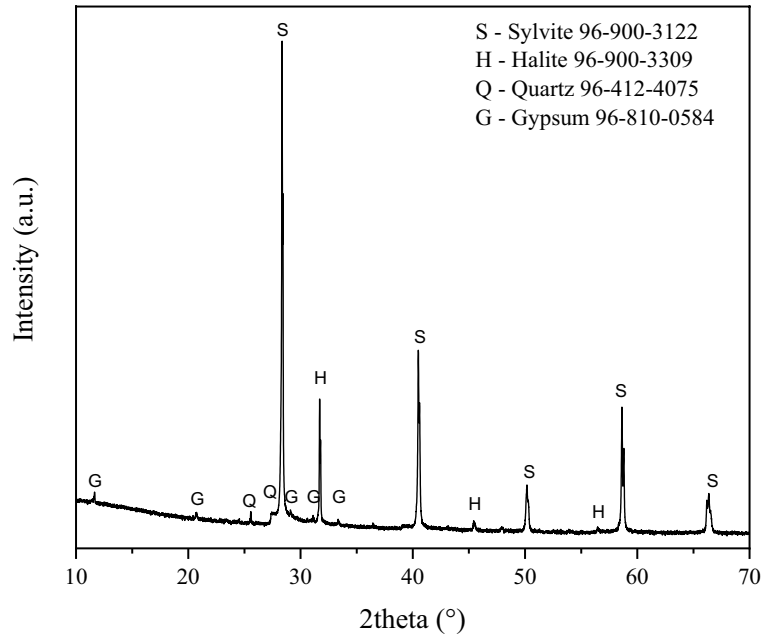

Fig. 9 XRD pattern of CBPD residue after centrifuge drying

Table 3 Comparison with previous literature on direct aqueous mineralisation conducted on cement bypass and kiln dust

Direct aqueous mineralisation									
Bibliography	Material	CaO (%)	L/S	P (atm)	Temperature (°C)	Time (h)	CO_2 flowrate (L/min)	CO_2 uptake (%)	η_{ca} (%)
[17]	CBPD	68	0.6	1	20	1	0.2	13	25
			100	1	20	1	0.2	15	28
[46]	CKD	46	0.1	2	20	72	n/a	12	41
	CBPD	66	0.1	2	20	72	n/a	26	51
This study	CBPD	39	3	1	20	1	2.5	20*	65
			3	1	40	1	2.5	25	82

*Calculated with Eq. (8) considering the same Δm obtained for CBPD12

[47] identified the presence of water as essential for achieving a high carbonation degree, they also observed that L/S ratios exceeding 20 could inhibit the carbonation reaction. In particular, the presence of excessive water resulted in the formation of a mass transfer barrier, which in turn lowered the ionic strength and decreased the rate of Ca^{2+} dissolution. Therefore, the superior outcome observed in this study at room temperature is consistent with previous literature, particularly given that an elevated CO_2 flow rate is also associated with an enhanced carbonation degree. Despite the use of an open system, the carbonation degree achieved in this study surpassed previous literature data. The considerable quantity of captured CO_2 substantiates the viability of this material for utilisation in carbon capture and utilisation (CCU) technologies. Additionally, this straightforward mineralisation technique is highly promising and has the potential to facilitate an integrated industrial process for CCU. Moreover, a reduction in KCl content during accelerated carbonation could enhance the reuse of carbonated CBPD, thereby upcycling this by-product.

4 Conclusions

The objective of this study was to investigate the accelerated aqueous carbonation of cement bypass dust, with particular attention paid to the influence of temperature and the efficiency with which salt is removed. The efficacy of various CO_2 quantification techniques was evaluated, and the findings were contextualised within the existing literature.

- The mineral composition of the CBPD was also studied, and it was found that the material contained significant quantities of high-reactive lime (CaO) and portlandite ($Ca(OH)_2$). These components underwent carbonation, resulting in a substantial increase in calcium carbonate content. The presence of KCl salt, as confirmed by both XRD and XRF analyses, presented a challenge in evaluating the COv uptake.
- The Response Surface Methodology was employed to construct an experimental design for the evaluation of the CO_2 content capacity of CBPD and the examination of the individual and joint effects of the operating parameters of time and temperature on the uptake. The experimental results demonstrated a considerable influence of the examined variables on the CO_2 content, which was observed to range between 14 and 24%. While the results were satisfactory, further investigation into additional operational parameters, such as the liquid-to-solid ratio, pressure, and CO_2 flow rate, could enhance the study. The present study investigated the accelerated aqueous carbonation of cement bypass dust with focus on the effect of temperature and the efficiency in terms of salt removal. Different CO_2 quantification methods were compared, and comparison with literature was provided.
- A modified formula for calculating the CO_2 uptake and the carbonation degree was implemented to consider the mass variations occurring during the mineralisation process, which are due to the hydration of calcium silicate species and the separation of salts. The CO_2 uptake was calculated for a single experimental point, namely 40 °C and 60 min, resulting in 24.1%. Had mass variations been neglected, the calculations would have yielded an error of + 3.6%.

The mass of KCl and NaCl removed by this aqueous carbonation process was approximately 18.5% of the initial mass of the sample. It would be beneficial to further investigate and improve this aspect of the process, particularly in light of the potential for reuse of the material. The high CO_2 storage capacity and the proximity of the material's production to the CO_2 emissions of a cement plant indicate that developing a carbon capture and utilisation technology may be a relatively straightforward process. Further investigation will be conducted on the potential reuse of carbonated CBPD as a supplementary cementitious material, with the aim of developing a more robust carbon capture, storage and utilisation technology.

Acknowledgements This research activity has been funded by the European Union for the PON "Ricerca e Innovazione" 2014-2020 Azione IV.4—REACT EU projects (DM 1061) and by CRH. The authors would like to express their gratitude to the Safety of Infrastructures and Constructions (SISCON) laboratory for providing the instrumentation for thermal analysis.

Funding Open access funding provided by Politecnico di Torino within the CRUI-CARE Agreement.

Declarations

Conflict of interest The authors declare that they have no conflict of interest.

References

1. Coppola L, Bellezze T et al (2023) New materials and technologies for durability and conservation of building heritage. Materials 16:1190. https://doi.org/10.3390/MA16031190

2. Cembureau, The European cement association-Activity Report, 2019.
3. USGS, Mineral Commodity Summaries, (2021). https://www.usgs.gov/centers/national-minerals-information-center/cement-statistics-and-information (accessed on 16/10/2023).
4. Annual CO_2 emissions from cement, (n.d.). https://ourworldindata.org/grapher/annual-co2-cement (accessed on 16/10/20233).
5. EPA U.S. Environmental Protection Agency, Report to congress on cement kiln dust, EPA-530-R-94–001, 1993.
6. Sturm G, Galichet B (2012) The Redudust project – an innovative solution for treatment of bypass-dust., Cement. International 10:60–65
7. Heikal M, Aiad I, Helmy IM (2002) Portland cement clinker, granulated slag and by-pass cement dust composites. Cem Concr Res 32:1805–1812. https://doi.org/10.1016/S0008-8846(02)00867-0
8. J. Saunders, T. Suzuki, N. Tamura, S. Saito, Recovering Potassium Salt for Fertiliser Use, Taiheiyo Cem. Kenkyu Hokoku 162 (2012) 37–42. https://jglobal.jst.go.jp/en/detail?JGLOBAL_ID=201102214063995843 (accessed on 16/10/2023).
9. BS EN 197–1(2011) Cement Composition, specifications and conformity criteria for common cements - European Standards, European Committee For Standardisation, 2011.
10. Taha R, Al-Rawas A, Al-Harthy A, Al-Siyabi H (2001) Use of cement by-pass dust in soil stabilization. Eng J Uni Qatar 14:61–76
11. Taha R, Al-Rawas A, Al-Harthy A, Qatan A (2002) Use of cement bypass dust as filler in asphalt concrete mixtures. J Mater Civ Eng 14:338–343. https://doi.org/10.1061/(ASCE)0899-1561(2002)14:4(338)
12. Emery JJ (1980) Stabilizing industrial sludge for fill applications. 7th International Congress on the Chemistry of Cement. CEREC, Paris, pp 644–648
13. E.M. Sipple, J. Mullner, A green building in a grey cement plant – Transforming bypass dust into industrial salt with the ReduDust Process, Rohoznik (SVK), 2016. https://www.atec-ltd.com/images/Redudust_ZKG_11.pdf (accessed on 27/11/2023).
14. Bonfante F, Ferrara G, Humbert P, Garufi D, Tulliani J-MC, Palmero P (2024) CO_2 sequestration through aqueous carbonation of electric arc furnace slag. J Adv Concr Technol 22:207–218. https://doi.org/10.3151/JACT.22.207
15. Huntzinger DN, Gierke JS, Kawatra SK, Eisele TC, Sutter LL (2009) Carbon dioxide sequestration in cement kiln dust through mineral carbonation. Environ Sci Technol 43:1986–1992. https://doi.org/10.1021/es802910z
16. Huntzinger DN, Gierke JS, Sutter LL, Kawatra SK, Eisele TC (2009) Mineral carbonation for carbon sequestration in cement kiln dust from waste piles. J Hazard Mater 168:31–37. https://doi.org/10.1016/J.JHAZMAT.2009.01.122
17. Araizi PK, Hills CD, Maries A, Gunning PJ, Wray DS (2016) Enhancement of accelerated carbonation of alkaline waste residues by ultrasound. Waste Manage 50:121–129. https://doi.org/10.1016/J.WASMAN.2016.01.006
18. Pan S-Y, Shah KJ, Chen Y-H, Wang M-H, Chiang P-C (2017) Deployment of accelerated carbonation using alkaline solid wastes for carbon mineralization and utilization toward a circular economy. ACS Sust Chem Eng. https://doi.org/10.1021/acssuschemeng.7b00291
19. Chang EE, Chen CH, Chen YH, Pan SY, Chiang PC (2011) Performance evaluation for carbonation of steelmaking slags in a slurry reactor. J Hazard Mater 186:558–564. https://doi.org/10.1016/J.JHAZMAT.2010.11.038
20. Baciocchi R, Costa G, Di Gianfilippo M, Polettini A, Pomi R, Stramazzo A (2015) Thin-film versus slurry-phase carbonation of steel slag: CO_2 uptake and effects on mineralogy. J Hazard Mater 283:302–313. https://doi.org/10.1016/j.jhazmat.2014.09.016
21. Steinour HH (1959) Some effects of carbon dioxide on mortars and concrete-discussion. J Am Concr Inst 30:905–907
22. Bezerra MA, Santelli RE, Oliveira EP, Villar LS, Escaleira LA (2008) Response surface methodology (RSM) as a tool for optimization in analytical chemistry. Talanta 76:965–977. https://doi.org/10.1016/j.talanta.2008.05.019
23. Ferrara G, Belli A, Keulen A, Tulliani J-M, Palmero P (2023) Testing procedures for CO_2 uptake assessment of accelerated carbonation products: experimental application on basic oxygen furnace steel slag samples. Constr Build Mater 406:133384. https://doi.org/10.1016/J.CONBUILDMAT.2023.133384
24. Humbert PS, Castro-Gomes JP, Savastano H (2019) Clinker-free CO_2 cured steel slag based binder: optimal conditions and potential applications. Constr Build Mater 210:413–421. https://doi.org/10.1016/J.CONBUILDMAT.2019.03.169
25. Mo L, Zhang F, Deng M (2016) Mechanical performance and microstructure of the calcium carbonate binders produced by carbonating steel slag paste under CO_2 curing. Cem Concr Res 88:217–226. https://doi.org/10.1016/J.CEMCONRES.2016.05.013
26. Mahoutian M, Shao Y, Mucci A, Fournier B (2015) Carbonation and hydration behavior of EAF and BOF steel slag binders. Mater Struct 48:3075–3085. https://doi.org/10.1617/s11527-014-0380-x
27. Moon EJ, Choi YC (2018) Development of carbon-capture binder using stainless steel argon oxygen decarburization slag activated by carbonation. J Clean Prod 180:642–654. https://doi.org/10.1016/J.JCLEPRO.2018.01.189
28. Liu G, Schollbach K, van der Laan S, Tang P, Florea MVA, Brouwers HJH (2020) Recycling and utilization of high-volume converter steel slag into CO_2 activated mortars – The role of slag particle size. Resour Conserv Recycl 160:104883. https://doi.org/10.1016/J.RESCONREC.2020.104883
29. Mahoutian M, Chaallal O, Shao Y (2018) Pilot production of steel slag masonry blocks. Can J Civ Eng 45:537–546. https://doi.org/10.1139/CJCE-2017-0603
30. Xuan D, Zhan B, Poon CS, Zheng W (2016) Carbon dioxide sequestration of concrete slurry waste and its valorisation in construction products. Constr Build Mater 113:664–672. https://doi.org/10.1016/J.CONBUILDMAT.2016.03.109
31. Kaddah F, Amiri O, Ranaivomanana H, Roziere E (2023) Accelerated carbonation of recycled concrete aggregates

and model materials. RILEM Bookseries 44:572–580. https://doi.org/10.1007/978-3-031-33187-9_53/COVER
32. Unluer C, Al-Tabbaa A (2014) Enhancing the carbonation of MgO cement porous blocks through improved curing conditions. Cem Concr Res 59:55–65. https://doi.org/10.1016/J.CEMCONRES.2014.02.005
33. Librandi P, Costa G, De Souza ACB, Stendardo S, Luna AS, Baciocchi R (2017) Carbonation of steel slag: testing of the wet route in a pilot-scale reactor. Energy Pro 114:5381–5392. https://doi.org/10.1016/J.EGYPRO.2017.03.1674/REFERENCES
34. Zhang D, Ghouleh Z, Shao Y (2017) Review on carbonation curing of cement-based materials. J CO2 Util 21:119–131. https://doi.org/10.1016/j.jcou.2017.07.003
35. Nielsen P, Quaghebeur M (2023) Determination of the CO_2 uptake of construction products manufactured by mineral carbonation. Minerals 13(1079):13. https://doi.org/10.3390/MIN13081079
36. Rossi TM, Campos JC, Souza MMVM (2020) Synthesis and characterization of hydrocalumite: influence of aging conditions on the structure, textural properties, thermal stability, and basicity. Clays Clay Miner 68:273–286. https://doi.org/10.1007/s42860-019-00049-6
37. Alonso C, Fernandez L (2004) Dehydration and rehydration processes of cement paste exposed to high temperature environments. J Mater Sci 39:3015–3024. https://doi.org/10.1023/B:JMSC.0000025827.65956.18/METRICS
38. Broström M, Enestam S, Backman R, Mäkelä K (2013) Condensation in the KCl–NaCl system. Fuel Process Technol 105:142–148. https://doi.org/10.1016/J.FUPROC.2011.08.006
39. Csizmadia J, Balázs G, Tamás FD (2001) Chloride ion binding capacity of aluminoferrites. Cem Concr Res 31:577–588. https://doi.org/10.1016/S0008-8846(01)00458-6
40. Suryavanshi AK, Narayan Swamy R (1996) Stability of Friedel's salt in carbonated concrete structural elements. Cem Concr Res 26:729–741. https://doi.org/10.1016/S0008-8846(96)85010-1
41. Goñi S, Guerrero A (2003) Accelerated carbonation of Friedel's salt in calcium aluminate cement paste. Cem Concr Res 33:21–26. https://doi.org/10.1016/S0008-8846(02)00910-9
42. W. Ashraf, J. Olek, V. Atakan, A Comparative Study of the Reactivity of Calcium Silicates during Hydration and Carbonation Reactions, in: 14th International Congress on the Chemistry of Cement (ICCC 2015), Beijing, China, 2015.
43. Czapik P, Zapała-Sławeta J, Owsiak Z, Stępień P (2020) Hydration of cement by-pass dust. Constr Build Mater 231:117139. https://doi.org/10.1016/J.CONBUILDMAT.2019.117139
44. Peethamparan S, Olek J, Lovell J (2008) Influence of chemical and physical characteristics of cement kiln dusts (CKDs) on their hydration behavior and potential suitability for soil stabilization. Cem Concr Res 38:803–815. https://doi.org/10.1016/J.CEMCONRES.2008.01.011
45. Oral ÇM, Ercan B (2018) Influence of pH on morphology, size and polymorph of room temperature synthesized calcium carbonate particles. Powder Technol 339:781–788. https://doi.org/10.1016/J.POWTEC.2018.08.066
46. Gunning PJ, Hills CD, Carey PJ (2010) Accelerated carbonation treatment of industrial wastes. Waste Manage 30:1081–1090. https://doi.org/10.1016/J.WASMAN.2010.01.005
47. Chang EE, Pan SY, Chen YH, Chu HW, Wang CF, Chiang PC (2011) CO_2 sequestration by carbonation of steelmaking slags in an autoclave reactor. J Hazard Mater 195:107–114. https://doi.org/10.1016/J.JHAZMAT.2011.08.006